*Acta Cryst.* (1980). A**36**, 592–600

# Electron Diffraction Intensities from Bent Molecular Organic Crystals

BY DOUGLAS L. DORSET

*Molecular Biophysics Department, Medical Foundation of Buffalo Inc., 73 High Street, Buffalo, New York* 14203, *USA*

(*Received* 30 *November* 1979; *accepted* 14 *February* 1980)

## Abstract

The mosaic model for thin molecular organic microcrystals does not adequately account for the electron diffraction intensities from them; nor is two-beam dynamical theory adequate. A bent-crystal model for diffraction proposed by Cowley [*Acta Cryst.* (1961), **14**, 920–927] explains well the observed electron diffraction intensities from orthorhombic paraffin microcrystals. In addition, previous verifications of *n*-beam dynamical electron scattering from these crystals (by fit of phase-grating structure-factor moduli to observed data and by the nonexistence of kinematical data at small electron wavelengths) are confirmed further by a good correspondence between calculated and observed *n*-beam data for increasing crystal thickness (*i.e.* monolayers of increasing-chain-length paraffins) and the change of continuously excited reciprocal-row intensities as the crystal is rotated about the axis. The better model for thin molecular organic microcrystals is therefore that of an elastically deformed perfect-crystal foil. Although *n*-beam dynamical effects can be demonstrated, the major limitation to crystal-structure analysis using intensity data from thin organic crystals is caused by the elastic bendings. This is particularly true if the crystals are solution grown and the longest unit-cell direction is therefore parallel to the incident beam. Epitaxial crystal growth, which minimizes bend effects to intensity data by forcing a shorter unit-cell axis to parallel the incident beam, effectively removes this apparent coherence restriction.

## Introduction

What conditions limit the use of electron diffraction intensity data from organic microcrystals for quantitative crystal-structure analysis? With numerous claims of such structural determinations in the literature, the prevailing viewpoint among many researchers is that there is almost no limitation.

The basis for this optimistic opinion largely rests on an early monograph on electron diffraction structure analysis (Vainshtein, 1964). In this work and in numerous other papers, it is proposed that the kinematical diffraction theory is a good model for electron diffraction from thin crystals. Microcrystals are reasoned to be imperfect – *i.e.* ensembles of mosaic blocks – and, given the disordered array of the mosaic, single diffracted beams are thought to be mostly excited in individual blocks. If the individual block size becomes large such that an appreciable fraction of the incident beam is diffracted, then the dynamical interactions are said to be well explained by two-beam theory (Vainshtein, 1956*a*).

The assumption of mosaicity in microcrystals persists along with the applications of two-beam theory to electron diffraction structure analysis (Imamov, 1976). In the polymer field, for example, single crystals of polyethylene are proposed to be composed of colloidal units some 300 Å in diameter (Hosemann, Wilke & Balta Calleja, 1966). Such blocks have not been observed in diffraction-contrast electron micrographs (Thomas, Sass & Kramer, 1974). However, as Buerger (1960) pointed out, Darwin never meant to imply the actual physical presence of such an array and a search for their presence *qua* blocks may be meaningless. The mosaic nature of a crystal depends on the *concentration* of defects in them and there is no doubt that suitable defects have been observed in these crystals (Bassett, 1964; Holland, 1964; Holland & Lindenmeyer, 1965; Holland, Lindenmeyer, Trivedi & Amelinckx, 1965; White, 1973, 1974; Dorset, 1978).

The derivation of the correct diffraction model for organic microcrystals demands that the defect concentration of the crystals and their major deformations be known. In sharp contrast with the above assumptions, Cowley (1975) has stated that the actual number of mosaic blocks in the electron beam path should be very small and that strong dynamical scattering can occur within these domains. Experimental determinations of defect occurrences in paraffinic crystals (Dorset, 1978) have also shown the concentration to be small. Two-beam dynamical theory, although giving an improved fit of calculated and observed electron diffraction data for paraffinic crystals (Li, 1963) does not explain specific beam intensity changes nearly as

0567-7394/80/040592-09$01.00 

well as an *n*-beam calculation (Dorset, 1976*a*). Also, there is a good correlation of intensity data from paraffin polycrystalline textures (Vainshtein, Lobachev & Stasova, 1958) to those from single crystals (Dorset, 1976*a*) indicating the same sort of dynamical interactions to be operational in the specimen type once envisioned to guarantee kinematical scattering (Vainshtein, 1956*b*).

It is the purpose of this paper to demonstrate further that thin organic microcrystals used for electron diffraction experiments can be regarded as nearly perfect. *N*-beam dynamical theory is shown, therefore, to be a more valid model of the electron scattering than two-beam theory. (When many diffracted beams are excited simultaneously, the latter two-beam theory requires an experimentally unjustified mosaic structure as outlined above to account for the independence of all diffracted beams.) The major crystal deformation, elastic bending, is shown to have a marked effect on the diffracted intensities in addition to *n*-beam effects and, based on experiments with simple paraffin crystals, the optimal use of electron diffraction intensities for crystal-structure analysis is defined.

## Experimental

### *Samples*

Thin crystals of several even-chain *n*-paraffins, *i.e.* *n*-tetracosane, $C_{24}H_{50}$ (Aldrich Chemical Co. Inc., Milwaukee, WI), *n*-hexacosane, $C_{26}H_{54}$ (Eastman Organic Chemicals, Rochester, NY), *n*-octacosane, $nC_{28}H_{58}$ (Aldrich Chemical Co. Inc., Milwaukee, WI), *n*-dotriacontane, $nC_{32}H_{66}$ (Eastman Organic Chemicals, Rochester, NY), *n*-hexatriacontane, $C_{36}H_{74}$ (Aldrich Chemical Co. Inc., Milwaukee, WI), *n*-tetracontane, $C_{40}H_{82}$ (Pfaltz & Bauer Inc., Stamford, CT), and *n*-tetratetracontane, $C_{44}H_{90}$ (Supelco Inc., Bellefonte, PA) were grown as the orthorhombic polymorph (Teare, 1959) by rapid evaporation of dilute hexane solutions onto carbon–Formvar-covered electron-microscope grids.

Monolayer crystals of a low-molecular-weight polyethylene (Polysciences Inc., Warrington, PA) were also obtained. Although sold as molecular weight 1000, an X-ray diffraction spacing at 117 Å revealed the mean chain length to be longer (*ca* 91 C atoms). Other experiments were done on crystals of *n*-hexatriacontane epitaxially grown from naphthalene by the procedure of Fryer (1980).

### *Electron microscopy and diffraction*

The electron microscopes used for this work were a JEOL JEM-100B (operated at 100 kV) equipped with a side-entry goniometer stage and a JEOL JEM-100U (operated at 100 kV). Most of the experiments were carried out on the first instrument. Usual precautions were taken to minimize radiation damage to the specimen (Dorset, 1976*a*).

In the experiments, a low-magnification (6700×) bright-field image was taken after each selected-area (16 μm diameter at specimen) electron diffraction pattern in order to estimate the crystal thickness. Evaluation of this thickness for solution-grown crystals is easily accomplished by counting the number of monomolecular layers in the characteristically terraced lozenge crystals (see Dawson & Vand, 1951) and knowing the monolayer thickness for a given chain length (Nyburg & Potworowski, 1973). Electron diffraction intensities from the patterns on Kodak X-ray film were obtained from them by use of a Joyce–Loebl Mark IIIC flat-bed microdensitometer and integrating under the scan peaks.

### *Computations*

Structure-factor calculations, *n*-fold self-convolutions of phased structure factors and multislice dynamical calculations were done on a PDP 11/45 computer. Doyle–Turner (1968) electron-scattering factors were used. All other calculations described in this paper were carried out by hand with the aid of a programmable calculator (Hewlett–Packard HP-67).

## I. *Crystal bending*

(*a*) *Orthorhombic paraffin structure.* A review of the crystal structure of orthorhombic *n*-paraffins (Teare, 1959) is given here in order that the following arguments based on this will be clear. As is shown by the (010) and (100) projections in Fig. 1, the unit cell of this structure is a bilayer made up of monolayers packing in the so-called $O_\perp$ subcell which is the crystalline aggregation of the methylene zig-zag repeat (Abrahamsson, Dahlén, Löfgren & Pascher, 1978), which is illustrated in Figs. 1 and 2(*a*). In order that the methyl end-plane packing energies of the contiguous monolayers may be minimized, the monolayers must be displaced from one another as is shown by the structure in Figs. 1 and 2(*b*). It is also possible to grow monolayer crystals of these paraffins which will result in the (001) projection shown in Fig. 2(*a*) – *i.e.* the projection is identical to the subcell. For the monolayer crystals the unit-cell repeat along the chain is the zig-zag distance of 2·54 Å. For the multilayer crystals, the unit-cell repeat in this direction is larger; the dimension for any paraffin given by Nyburg & Potworowski (1973). The model compound used for bend calculations below is $nC_{16}H_{34}$ which would have a 'long spacing' of 44·33 Å.

The (*uv*0) Patterson maps of monolayer and multilayer orthorhombic paraffin crystals are easily obtained by graphical autocorrelation (see Cowley,

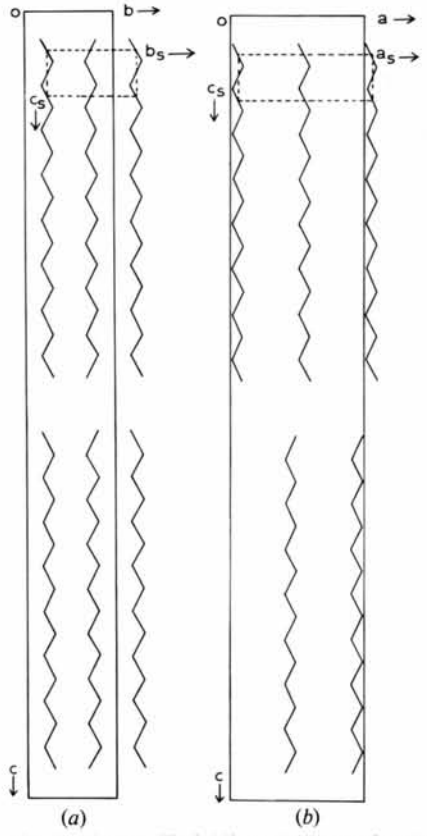


Fig. 1. The (*a*) (010) and (*b*) (100) projections of orthorhombic paraffins after Teare (1959), showing disposition of molecular monolayers in the unit cell. For these structures $a = 7{\cdot}4$, $b = 5{\cdot}0$, $c = (2{\cdot}54n + 3{\cdot}693)$ Å, where $n$ is the number of carbons in the chain (see Nyburg & Potworowski, 1973). The 'subcell' of the zig-zag repeat is also indicated.

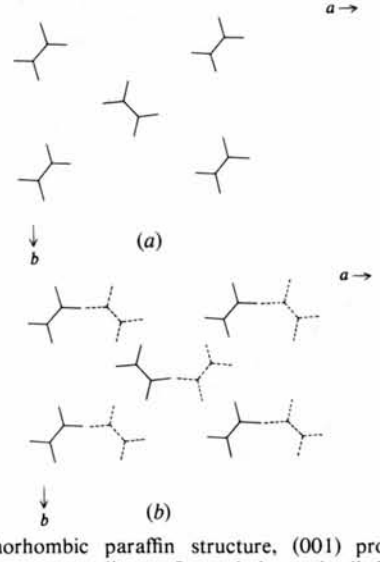


Fig. 2. Orthorhombic paraffin structure, (001) projection. (*a*) Monolayer corresponding to $O_\perp$ methylene subcell. Carbon atom coordinates $x/a = 0{\cdot}039$, $y/b = 0{\cdot}064$ (Teare, 1959), plane group *pgg*; (*b*) bilayer showing shifted second layer, carbon atom coordinates; C(1) $x/a = 0{\cdot}014$, $y/b = 0{\cdot}186$; C(2) $x/a = 0{\cdot}092$, $y/b = 0{\cdot}314$, plane group *pgm* (a *pgg* projection can also be defined by a shift of origin).

1975, p. 94) of Figs. 2(*a*),(*b*). Similarly, ($u0w$) and ($0vw$) Pattersons are obtained by autocorrelations of monolayers and bilayers of Fig. 1. Typical 'self-image' autocorrelations of paraffins have been shown by Stout & Jensen (1968). For the bilayer case, the ($uv0$) Patterson is essentially composed of two monolayer components. One component with origin (0,0) is composed of vectors within a monolayer whereas the other with origin at (0·106, 0·50) is composed of vectors between monolayers. The three-dimensional Patterson contains columns of peaks originating from the planes at $w = 0$, $w = \frac{1}{2}$, which diminish in weight as they occur further from the respective origins.

For untilted solution-grown crystals of orthorhombic *n*-paraffins (Fig. 3), the electron beam impinges onto the (001) face and is parallel to the long chain axes, giving the characteristic ($hk0$) diffraction pattern in Fig. 4(*a*), if it is a monolayer crystal. Bilayer crystals would give a diffraction pattern *similar to* Fig. 4(*b*) due to the displacement of monolayers in the crystal structure.

Fourier transformation of the Patterson function gives the diffracted intensity. Since the symmetry of the bilayer (001) projection is *pgm* [using the Teare (1959)

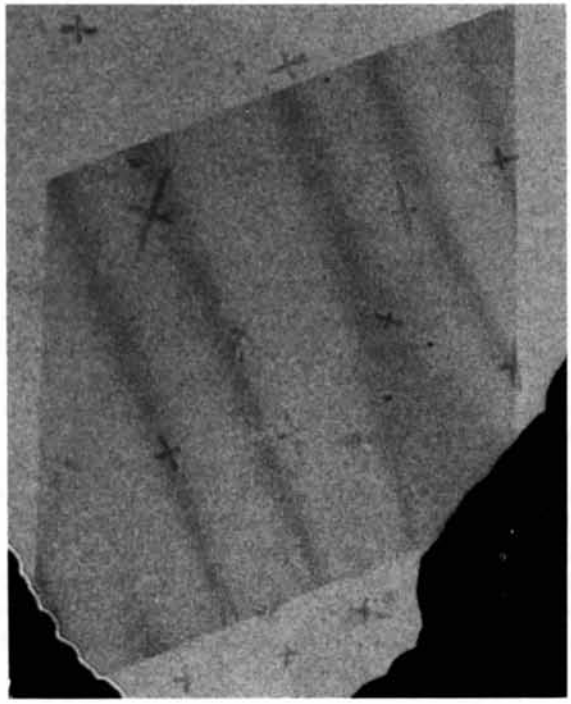

Fig. 3. Monolayer crystal of *n*-tetracontane showing characteristic lozenge shape and bend contours (bright-field image). The contours in this image indicate a cylindrical bend here but other images indicate that the bends can be sections of spheres or irregular. Small crosses are dendritic crystals, showing preferred growth along [100] and [010].

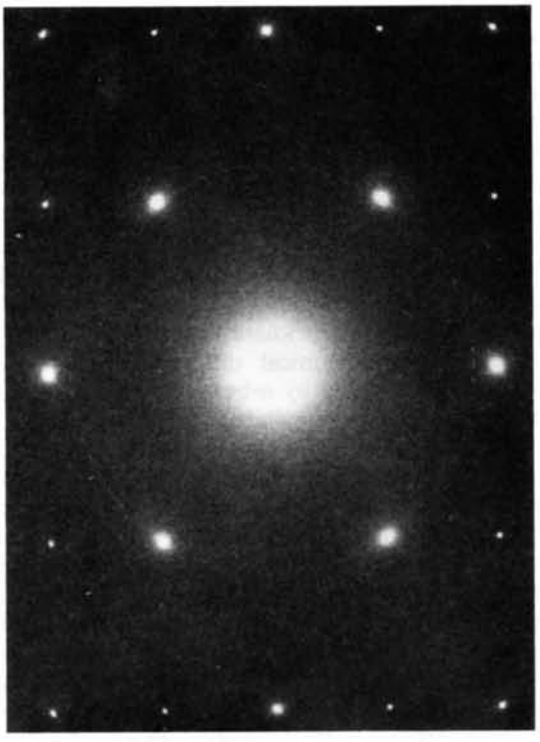

(*a*)

(*b*)

Fig. 4. (*a*) Characteristic *hk*0 electron diffraction pattern from an orthorhombic paraffin monolayer; note $I_{110} \simeq I_{200}$. (*b*) Electron diffraction pattern with small-angle data characteristic of bilayer unit cell; note $I_{110} < I_{200}$.

origin], the (*uv*0) Patterson has *pmm* symmetry and the trigonometric part of the intensity calculation is

$$\begin{aligned} A_{hk} &= \sum_{x,y} \{\cos 2\pi hx \cos 2\pi ky + \cos 2\pi h(x + 0{\cdot}106) \\ &\quad \times \cos 2\pi k(y + 0{\cdot}5)\} \\ &= \sum_{x,y} \{\cos 2\pi hx \cos 2\pi ky + [(-1)^k \\ &\quad \times \cos 0{\cdot}212\ \pi h \cos 2\pi hx \cos 2\pi ky \\ &\quad - (-1)^k \sin 0{\cdot}212\pi h \sin 2\pi hx \cos 2\pi ky]\}. \quad (1) \end{aligned}$$

The term in square brackets gives the change of the monolayer-type diffracted intensities due to the contribution from the origin-shifted second monolayer Patterson component.

(*b*) *Bending and the diffraction model.* Examples of bending have been shown for thin microcrystals of paraffins and paraffin-like compounds with diffraction-contrast micrographs in a previous paper (Dorset, 1978) giving measured values up to $\pm 5{\cdot}0°$. Bends are also seen in the monolayer orthorhombic paraffin crystal in Fig. 3. Experiments on single crystals with several selected areas sampled show the overall bending to be irregular but, on the other hand, large fractions of the crystal have a regular bend.

The diffraction model used for the intensity calculations was derived by Cowley (1961) and was already used (Dorset, 1978) for the monoclinic paraffin case. The total Patterson function is modified by the bending as shown in Cowley's expression. The resultant intensity $I(\mathbf{s})$ is defined by

$$I(\mathbf{s}) = \sum_i W_i(\mathbf{s}) \exp(2\pi i \mathbf{r}_i . \mathbf{s}) \exp[-(\pi^2/\sigma^2)s^2 z_i^2]. \quad (2)$$

Here $W_i(\mathbf{s})$ is the 'scattering factor' evaluated at reciprocal vector $\mathbf{s}$ due to the Patterson peak $w_i(\mathbf{r})$ with

Table 1. *Kinematical data for bent monolayer crystals of n-hexatriacontane* ($B = 0$ Å$^2$)

| | $F_{kin}$ | $\lvert F_{kin}\rvert$ at ± bend | | | |
|---|---|---|---|---|---|
| *h k* 0 | 0° | 2·5° | 5·0° | 7·5° | 10·0° |
| 2 0 0 | 7·02 | 6·70 | 6·04 | 5·39 | 4·86 |
| 4 0 0 | 3·06 | 2·62 | 2·12 | 1·78 | 1·59 |
| 1 1 0 | 7·28 | 7·02 | 6·43 | 5·78 | 5·25 |
| 2 1 0 | −1·62 | 1·51 | 1·32 | 1·14 | 1·02 |
| 3 1 0 | 2·28 | 2·03 | 1·68 | 1·44 | 1·27 |
| 4 1 0 | −1·20 | 1·02 | 0·81 | 0·68 | 0·60 |
| 0 2 0 | 3·80 | 3·46 | 2·92 | 2·52 | 2·25 |
| 1 2 0 | −1·48 | 1·34 | 1·12 | 0·96 | 0·85 |
| 2 2 0 | 1·36 | 1·20 | 0·98 | 0·84 | 0·73 |
| 3 2 0 | −1·72 | 1·46 | 1·17 | 0·99 | 0·86 |
| 4 2 0 | 0·48 | 0·39 | 0·30 | 0·24 | 0·22 |
| 1 3 0 | 1·76 | 1·46 | 1·15 | 0·98 | 0·86 |
| 2 3 0 | −1·74 | 1·42 | 1·11 | 0·94 | 0·82 |
| 3 3 0 | 0·60 | 0·48 | 0·37 | 0·30 | 0·26 |
| 4 3 0 | −1·34 | 1·03 | 0·78 | 0·66 | 0·57 |

vector length $|\mathbf{r}_i|$. The vector $\mathbf{r}_i$ has a component $z_i$ in the electron beam direction. Bend modulation of (2) is given by $\sigma$ which is the inverse of total bending in radians. By (2), not only will the effect of bending be large for Patterson vectors with large $z_i$, it will also be more in evidence for reflections at larger reciprocal distance $s$.

Intensity calculations for bent orthorhombic paraffin monolayers use the first cos $2\pi hx$ cos $2\pi ky$ trigonometric term of (1). Again, the weight of the eclipsed Patterson peaks in the calculation is most attenuated for wide-angle reflection. Results of the calculation for monolayers is given in Table 1.

For the bilayer crystals, Patterson peak weights [with trigonometric terms of the bracketed part of (1)] at longest vector lengths are attenuated most by bending, giving results as shown in Table 2. These calculations readily explain the previous observation for slightly bent crystals (Dorset, 1977*a*) that small-angle intensities appear to originate from the true bilayer unit cell and wide-angle intensities seem to be due to a monolayer alone.

## II. *Dynamical scattering*

(*a*) *Verification of n-beam scattering.* As stated in the *Introduction*, there is evidence for *n*-beam dynamical scattering from thin organic crystals. The first evidence found was that an *n*-beam calculation gives a very good fit to observed structure-factor moduli in a highly specific way not seen in two-beam calculations. This was shown for two cases, the orthorhombic paraffins (Dorset, 1976*a*) and for an oligomer of polytetrafluoroethylene (Dorset, 1977*b*).

In the phase-grating approximation (Cowley & Moodie, 1959), two variables are shown to affect the strength of dynamical interactions, *viz* accelerating voltage (electron wavelength) and crystal thickness. Experiments on thin orthorhombic *n*-hexatriacontane crystals giving (*hk*0) electron diffraction intensities at an accelerating voltage between 300 and 1000 kV (Dorset, 1976*b*) have shown that the primary extinction correction suggested by Honjo & Kitamura (1957) is invalid. Kinematical intensity values are not reached at high electron-accelerating voltages.

Instead of varying accelerating voltage, one can also change crystal thickness. Growth of monolayer paraffin crystals from $n\mathrm{C}_{24}\mathrm{H}_{50}$ to $n\mathrm{C}_{44}\mathrm{H}_{90}$ effectively changes the crystal thickness from 32·33 to 57·73 Å. Ratios of the dynamical diffracted-beam structure factors most changed by *n*-beam scattering, *i.e.* $|F_{220}|$ and $|F_{310}|$, to a less-altered reflection, $|F_{120}|$, are plotted in Fig. 5. These values were obtained from a phase-grating calculation (see Dorset, 1976*a*) and/or a full multislice dynamical calculation. The ratio of these moduli to a structure factor nearby in reciprocal space is used in order to minimize the effects of variable bending in diffraction patterns from several crystals on a grid. This expedient is only partially successful. With a small crystal bend the effective coherent scattering length can become less than the chain length, as shown above. This accounts for larger standard deviation in measured mean relative structure factors for longer-chain alkanes seen in Fig. 5. Measured moduli for the polyethylene sample – not shown in Fig. 5 – are less than the values predicted for unbent crystals, *i.e.* $|F_{310}|/|F_{120}|$ obs. 2·11 ± 0·54, calc. 2·86; $|F_{220}|/|F_{120}|$ obs. 1·72 ± 0·29, calc. 2·70. Observed values of these relative structure factors are also indicated in this plot and are seen to correspond well to the theoretical values. No such change in relative structure factors is predicted by either kinematical or

Table 2. *Kinematical data for bent bilayer crystals of n-hexatriacontane* ($B$ = 0 Å$^2$) [*scaled to subcell structure factors by* $I_{020}$ (*subcell*) = $I_{020}$ (*unit cell*)]

| | $F_{kin}$ | $\lvert F_{kin}\rvert$ at ± bend | | | |
|---|---|---|---|---|---|
| *hk*0 | 0° | 2·5° | 5·0° | 7·5° | 10·0° |
| 2 0 0 | 5·52 | 5·61 | 5·54 | 5·16 | 4·75 |
| 4 0 0 | 0·72 | 2·05 | 1·99 | 1·73 | 1·56 |
| 1 1 0 | −2·38 | 3·65 | 4·83 | 5·03 | 4·88 |
| 2 1 0 | 1·50 | 1·14 | 1·19 | 1·09 | 0·99 |
| 3 1 0 | −1·92 | 1·87 | 1·63 | 1·42 | 1·26 |
| 4 1 0 | 1·16 | 1·00 | 0·80 | 0·68 | 0·60 |
| 0 2 0 | −3·80 | 3·46 | 2·92 | 2·52 | 2·25 |
| 1 2 0 | 1·40 | 1·30 | 1·10 | 0·95 | 0·85 |
| 2 2 0 | −1·07 | 1·08 | 0·95 | 0·82 | 0·73 |
| 3 2 0 | 0·94 | 1·24 | 1·11 | 0·97 | 0·85 |
| 4 2 0 | −0·11 | 0·33 | 0·28 | 0·24 | 0·22 |
| 1 3 0 | 0·58 | 1·22 | 1·10 | 0·96 | 0·86 |
| 2 3 0 | −1·07 | 1·28 | 1·08 | 0·93 | 0·82 |
| 3 3 0 | 0·51 | 0·46 | 0·36 | 0·30 | 0·26 |
| 4 3 0 | −1·31 | 1·03 | 0·78 | 0·66 | 0·57 |

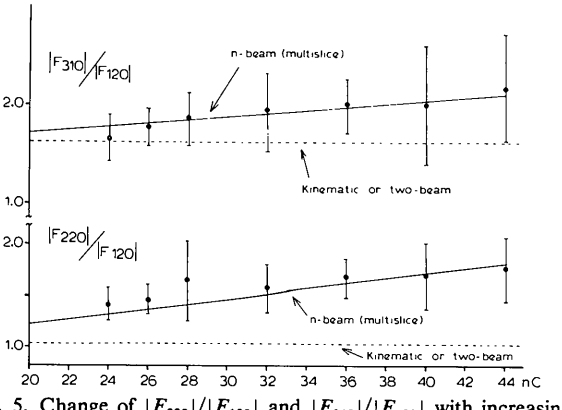


Fig. 5. Change of $|F_{220}|/|F_{120}|$ and $|F_{310}|/|F_{120}|$ with increasing thickness (*i.e.* number of 2·54 Å zig-zag repeats). Solid lines are derived from a phase-grating calculation and/or a full multislice calculation with input kinematical data calculated with temperature factor $B$ = 3·0 Å$^2$ (see Dorset, 1976*a*). Dashed lines indicate the results of kinematical or two-beam calculations (identical here because of the very large two-beam 'extinction distances' for these structures). Experimental points from actual diffraction patterns are indicated by points with error bars.

two-beam theory. This is a third verification of the validity of the *n*-beam scattering calculation.

In principle yet another method can be used to demonstrate the existence of *n*-beam dynamical scattering from these long-chain compounds. If the orthorhombic paraffin structure in Fig. 1 is rotated by 27° about the [100] (≃7·5 Å) crystallographic axis with concomitant slippage of long chain axes to give a flat methyl end plane, the monoclinic form of even paraffins is formed (see Shearer & Vand, 1956), which preserves the same side-to-side chain packing of the orthorhombic form. [Bend effects on diffraction from untilted monoclinic crystals were described in a previous paper (Dorset, 1978).] Again, a rotation of this structure about this axis by 27° gives the same diffraction pattern found for the untilted orthorhombic paraffins.

When the goniometer axis is coincident with the subcell *a* (≃7·5 Å) axis, the $(h00)_s$ layer-line reflections are continuously excited as the crystal is tilted. As shown by Cowley & Kuwabara (1962), the ratio of layer-line intensities for these continously excited reflections should change *only* if *n*-beam dynamical effects are in evidence. Numerous experiments were carried out with microcrystalline cetyl palmitate, a wax which assumes the monoclinic paraffin structure (Kohlhaas, 1938). The goniometer stage of the electron microscope was initially tilted by 27° and the grid was translated or rotated until a characteristic subcell *hk*0 pattern (Fig. 4*a*) was seen. As the crystal was tilted by 3° increments, its centered position with respect to the selected-area aperture was maintained by viewing a small bright-field image in a defocused diffraction pattern before the focused diffraction pattern was recorded. Between exposures the beam was translated away from the specimen by switching to deliberately misaligned 'dark-field' controls.

The plot in Fig. 6 indicates again that *n*-beam dynamical scattering effects are discernible in the diffraction from such long-chain compounds. It should be pointed out that in the numerous tilt series obtained from cetyl palmitate crystals, it was not possible to reproduce exactly this observed intensity change. However, several series gave the same trend in intensity change with tilt. Varations in diffraction from crystal to crystal are mostly due to irregular bending over the rather large selected area (>10 μm diameter) as is evidenced by disappearance of Friedel symmetry in some diffraction patterns of a tilt series, an effect which cannot be corrected by maintaining a fixed crystal position. Another source of error would be a slight precessing of the reciprocal axis about the goniometer tilt axis. Radiation damage, on the other hand, is negligible because of the very low beam current used, as well as the removal of the beam from the sample while it is tilted. The integrity of the crystal is indicated by the visualization of bend contours in the bright-field image after the tilt series.

(*b*) *n-beam dynamical scattering from a bent crystal.* It is difficult to combine the results of the kinematical model for bending with an *n*-beam dynamical calculation because structure-factor moduli obtained from the Patterson model in (2) are unphased. For the monolayer case where the carbon chain zig-zag repeat is the unit cell in the beam direction, there is no additional phase change due to shifted atomic positions for the untilted crystals. Hence it appears reasonable to use the moduli obtained from the bend calculation with

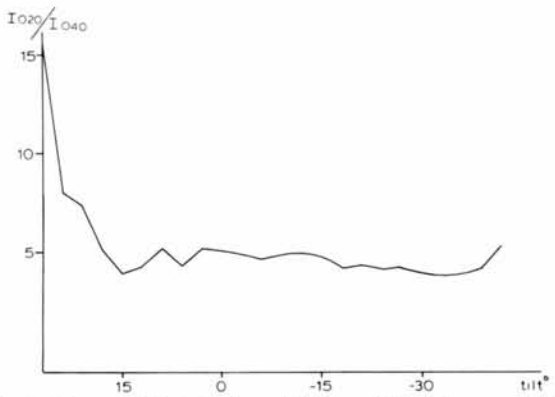


Fig. 6. Change of $I_{020}/I_{040}$ (here $[100]_{subcell}$ is $[010]_{unit\ cell} \simeq 7{\cdot}5$ Å) with crystal tilt around $[010]_{unit\ cell}$ for a single monoclinic crystal of cetyl palmitate.

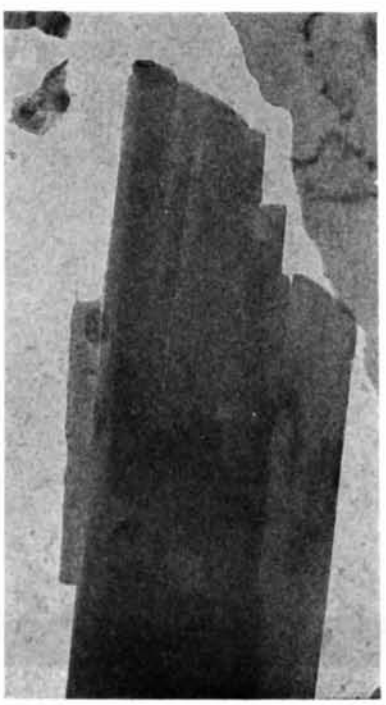

Fig. 7. Bright-field image of lath *n*-hexatriacontane crystals epitaxially grown in naphthalene. Calibration of image rotation to diffraction pattern (see Fig. 8) shows that molecular long-chain axes are normal to lath length.

the known monolayer phases to represent the average 'kinematical' structure. Such data for various bends were used in a phase-grating calculation for the monolayer to confirm the appearance of the dynamically increased $|F_{220}|$ and $|F_{310}|$ observed in experimental electron diffraction patterns.

It is not valid to use such an approximation for the bilayer case. The kinematical model for bending used above deals with the diminished weight of long-range Patterson vectors in intensity and, given the phase shifts due to translated successive molecular monolayers (Fig. 2), the results of the bend calculation cannot be used as an 'average kinematical structure' for a multislice calculation, which deals with successive thin layers (*e.g.* single zig-zags) in the crystal. An *n*-beam dynamical calculation for a bent crystal, therefore, will necessitate a rigorous consideration of a molecular packing model which has overall curvature, and is outside the present scope of this paper.

## III. *Electron diffraction from epitaxially grown crystals.*

As has been shown by Fryer (1980), *n*-paraffins epitaxially crystallized from naphthalene give laths (Fig. 7) which are *nearly* the (100) projection of the orthorhombic crystalline polymorph (Fig. 1). There appears to be some ambiguity in the nucleation of this structure in terms of rotation around the chain axis, but the 0*kl* pattern (Fig. 8) can be located by rotation about $c^*$ by a few degrees. As found with the solution-grown crystals (Fig. 3) there is again elastic bending, as evidenced by bend contours in diffraction-contrast images (Fig. 7) and by deviations from *mm* symmetry in the observed electron diffraction patterns.

It is most important to note that the zonal electron diffraction intensities now appear to originate from the whole unit cell. A comparison of observed 00*l* intensity data (from a crystal with good Friedel symmetry in this row) with calculated kinematical values (Table 3) shows close agreement. Quantitative comparison of the whole zonal data set to the kinematical data has not been made, because no 0*kl* pattern has been recorded yet which adequately satisfies *mm* symmetry in intensity. However, systematic absences for the (100) zone are correct as well as location of 0*kl* intensity maxima (see Teare, 1959). An attempt to use the 0*kl* data from the pattern schematized in Fig. 8 necessitated a different scale factor for each *k*-row of spots which increased with increasing *k*. The crystal in this example is thus slightly tilted about $c^*$ as well as being somewhat bent. This observation is predicted by the bending model given above. Epitaxial growth of the paraffin now places a *ca* 7·5 Å axis parallel to the incident electron beam instead of the much larger axis posited by solution growth. Since the longest Patterson vector components parallel to the incident beam for this projection are now no larger than 7·5 Å, the small bends in the microcrystalline laths will not cause apparent coherent diffraction from less than the unit

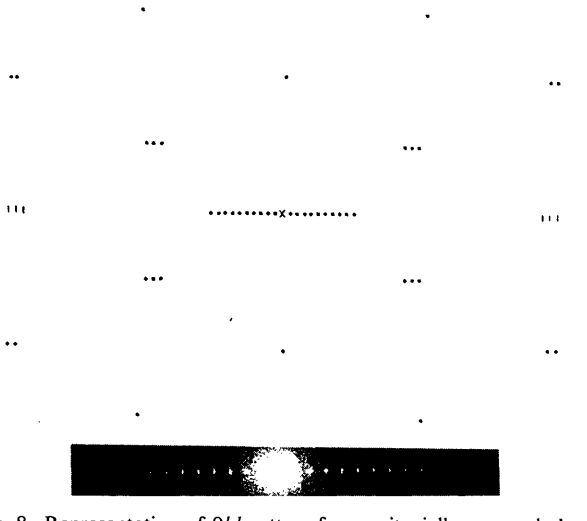

Fig. 8. Representation of 0*kl* pattern from epitaxially grown, lath-habit, *n*-hexatriacontane crystals. This pattern is rarely found for untilted crystals, but can be obtained by tilting the crystals a few degrees (*e.g.* 8°) about $c^*$. The most commonly found diffraction pattern is a 00*l* row (inset).

Table 3. *Comparison of observed and calculated electron diffraction data from epitaxially grown microcrystals of n-hexatriacontane*

Teare's (1959) *z*/*c* coordinates are used.

| (00*l*) | $\lvert F_{obs}\rvert$ | $\lvert F_{calc}\rvert$ $B = 6$ Å$^2$ |
|---|---|---|
| 6 | 3·14 | 3·46 |
| 8 | 3·11 | 3·36 |
| 10 | 3·11 | 3·26 |
| 12 | 3·32 | 3·12 |
| 14 | 3·05 | 2·48 |
| 16 | 3·08 | 2·81 |
| 18 | 3·08 | 2·63 |
| 20 | 2·49 | 2·47 |
| 22 | 2·43 | 2·28 |
| 24 | 2·15 | 2·08 |
| 26 | 2·03 | 1·91 |
| 28 | 1·94 | 1·73 |
| 30 | 2·18 | 1·53 |
| 32 | 1·54 | 1·37 |
| 34 | 1·29 | 1·19 |
| 36 | 1·29 | 1·04 |
| 38 | 1·14 | 0·87 |
| 40 | 1·29 | 0·73 |
| ⋮ | | |
| 72 | 1·57 | 2·15 |
| 74 | 6·65 | 6·92 |
| 76 | 2·68 | 4·79 |

$$R = \frac{\sum||F_{calc}| - k|F_{obs}||}{\sum k|F_{obs}|} = 0{\cdot}14.$$

cell. For example, at the *maximum* observed resolution of the paraffin 00*l* patterns, *i.e.* $d^* = 0{\cdot}80$ Å$^{-1}$ (0,0,76 reflection), a crystal would have to be bent more than $\pm 3°$ for any major intensity changes to be discerned because of this distortion. Comparison with Table 2 shows that appreciable changes are already observed for the solution-grown crystals over most of the pattern at this bend value. In other words, a crystal-structure determination with data from epitaxially grown crystals would give a true representation of the whole unit cell whereas a determination with data from solution-grown crystals would give (at best!) only a partial representation of the unit cell.

## Discussion

The experimental results given above support the thesis that thin molecular organic crystals used in electron diffraction experiments are nearly perfect. The major deviation from perfection is elastic bending and not the mosaicity imagined in earlier studies. An expression of crystal perfection is the observation of *n*-beam dynamical effects in the electron diffraction intensity data by at least four methods; therefore the use of two-beam arguments for correcting data from such crystals is incorrect. Since the $Z$ values for atoms in organic crystals are small, and if the crystals are suitably thin, diffracted intensities are near enough to their kinematical values to allow *ab initio* crystal-structure analysis (*e.g.* see Dorset & Hauptman, 1976; Dorset, Jap, Ho & Glaeser, 1979).

It is therefore important to note that the major restriction to crystal-structure analysis is not due to dynamical effects. Rather it is seen that the commonly observed elastic bending in microcrystals can cause seemingly bizarre changes in diffraction intensity, particularly if the unit-cell dimension parallel to the incident beam is large. This has been shown previously for an example where solution-grown crystals of long-chain molecules are packed so that chain axes are inclined to the major crystal plate face (Dorset, 1978) and is again demonstrated here for a case where these axes are normal to the major face. For solution-grown crystals of the unknown long-chain structure, the most favorable expectation is to locate the long-chain-axis direction in the crystal and then to identify the side to side packing of these chains from the electron diffraction intensity data. This has been done for a multitude of long-chain lipids in our laboratory, identifying chain packings representative of four methylene 'subcells' and a variety of chain inclinations. However, since interesting features of these crystal structures, which are expressed by long Patterson vectors (*e.g.* substituent groups and conformations of chains around them), are effectively invisible, there was always the specter of an incomplete structural elucidation due to the limitations imposed by bending.

It is fortunate that these compounds are amenable to epitaxial crystal growth and that the methodology derived by Fryer (1980) allows the crystal plate to be suitably large. In addition to the *n*-paraffin mentioned here, we have successfully crystallized a variety of representative structures including linear waxes, glycerides of varying polarity, and even phospholipids. All have given 'long spacings' in the electron diffraction patterns which either match previous X-ray powder diffraction results or the expected values of other observed polymorphic forms. Furthermore, as shown above, the diffraction data represent the total unit cell.

Thus there is no reason why complete long-chain organic crystal structures cannot be solved from electron diffraction intensity data. Indeed, the effective coherence-length restriction found in diffraction from bent solution-grown crystals can be used advantageously to elucidate the long-chain packing and this information can be used in the complete structural elucidation with epitaxially grown crystals.

The author would like to express his deep gratitude to Dr John R. Fryer, who described the details of this ingenious method for epitaxial growth of long-chain compounds. The author is also grateful for helpful technical assistance from Mrs Cynthia M. Stewart. Research was funded by Public Health Service Grant No. GM-21047 from the National Institute of General Medical Sciences and by National Science Foundation Grant Nos. PCM78-16041, and CHE79-16916.

## References

ABRAHAMSSON, S., DAHLÉN, B., LÖFGREN, H. & PASCHER, I. (1978). *Prog. Chem. Fats Other Lipids*, **16**, 125–143.
BASSETT, D. C. (1964). *Philos. Mag.* **10**, 595–615.
BUERGER, M. J. (1960). *Crystal-Structure Analysis*, pp. 197–198. New York: Wiley.
COWLEY, J. M. (1961). *Acta Cryst.* **14**, 920–927.
COWLEY, J. M. (1975). *Diffraction Physics*, pp. 341–342. Amsterdam: North-Holland.
COWLEY, J. M. & KUWABARA, S. (1962). *Acta Cryst.* **15**, 260–269.
COWLEY, J. M. & MOODIE, A. F. (1959). *Acta Cryst.* **12**, 360–367.
DAWSON, I. M. & VAND, V. (1951). *Proc. R. Soc. London Ser. A*, **206**, 555–562.
DORSET, D. L. (1976*a*). *Acta Cryst.* A**32**, 207–215.
DORSET, D. L. (1976*b*). *J. Appl. Phys.* **47**, 780–782.
DORSET, D. L. (1977*a*). *Z. Naturforsch. Teil A*, **32**, 1166–1172.
DORSET, D. L. (1977*b*). *Chem. Phys. Lipids*, **20**, 13–19.
DORSET, D. L. (1978). *Z. Naturforsch. Teil A*, **33**, 964–982.
DORSET, D. L. & HAUPTMAN, H. A. (1976). *Ultramicroscopy*, **1**, 195–201.
DORSET, D. L., JAP, B. K., HO, M.-H. & GLAESER, R. M. (1979). *Acta Cryst.* A**35**, 1001–1009.
DOYLE, P. A. & TURNER, P. S. (1968). *Acta Cryst.* A**24**, 390–397.

FRYER, J. R. (1980). In preparation.
HOLLAND, V. F. (1964). *J. Appl. Phys.* **35**, 3235–3241.
HOLLAND, V. F. & LINDENMEYER, P. H. (1965). *J. Appl. Phys.* **36**, 3049–3056.
HOLLAND, V. F., LINDENMEYER, P. H., TRIVEDI, R. & AMELINCKX, S. (1965). *Phys. Status Solidi*, **10**, 543–569.
HONJO, G. & KITAMURA, N. (1957). *Acta Cryst.* **10**, 533–534.
HOSEMANN, R., WILKE, W. & BALTA-CALLEJA, F. J. (1966). *Acta Cryst.* **21**, 118–123.
IMAMOV, R. M. (1976). In *Crystallographic Computing Techniques*, edited by F. R. AHMED, pp. 357–362. Copenhagen: Munksgaard.
KOHLHAAS, R. (1938). *Z. Kristallogr.* **98**, 418–438.
LI FAN-KHUA (1963). *Acta Phys. Sin.* **19**, 735–740.
NYBURG, S. C. & POTWOROWSKI, J. A. (1973). *Acta Cryst.* B**39**, 347–352.
SHEARER, H. M. M. & VAND, V. (1956). *Acta Cryst.* **9**, 379–384.
STOUT, G. H. & JENSEN, L. H. (1968). *X-ray Structure Determination. A Practical Guide*, p. 305. New York: Macmillan.
TEARE, P. W. (1959). *Acta Cryst.* **12**, 294–300.
THOMAS, E. L., SASS, S. L. & KRAMER, E. J. (1974). *J. Polym. Sci. Polym. Phys. Ed.* **12**, 1015–1022.
VAINSHTEIN, B. K. (1956*a*). *Sov. Phys.–Crystallogr.* **1**, 15–21.
VAINSHTEIN, B. K. (1956*b*). *Sov. Phys.–Crystallogr.* **1**, 117–122.
VAINSHTEIN, B. K. (1964). *Structure Analysis by Electron Diffraction*. Oxford: Pergamon.
VAINSHTEIN, B. K., LOBACHEV, A. N. & STASOVA, M. M. (1958). *Sov. Phys.–Crystallogr.* **3**, 452–459.
WHITE, J. R. (1973). *J. Polym. Sci. Polym. Phys. Ed.* **11**, 2173–2184.
WHITE, J. R. (1974). *J. Polym. Sci. Polym. Phys. Ed.* **12**, 2375–2391.

*Acta Cryst.* (1980). A**36**, 600–604

# Extinction Correction in White X-ray and Neutron Diffraction

BY S. TOMIYOSHI, M. YAMADA AND H. WATANABE

*The Research Institute for Iron, Steel and Other Metals, Tohoku University, Sendai, Japan*

(*Received* 19 *November* 1979; *accepted* 30 *January* 1980)

## Abstract

Extinction effects in white-beam X-ray and neutron diffraction are considered following the formulation developed for monochromatic-beam diffraction by Becker & Coppens [*Acta Cryst.* (1974), A**30**, 129–147]. In white-beam diffraction, a small deviation of the wavelength from the Bragg condition $\Delta\lambda$ is a variable which represents the line profile of the diffraction peaks, so that by using the new parameter $\Delta\lambda$ the theory is converted to one in white-beam diffraction. It is shown that for a convex crystal, primary extinction $y_p$ agrees with the results calculated already for monochromatic diffraction. The same relation is shown to hold in secondary extinction $y_s$. It is concluded that extinction theory derived for monochromatic diffraction is applicable without any modification in white-beam diffraction.

## 1. Introduction

Recently, crystal-structure studies using the white-beam diffraction method have taken a more and more important place because of the advance in energy-dispersive solid-state X-ray detectors in X-ray diffraction, and the increase in available pulsed-neutron sources in neutron diffraction. In order to obtain the structure factor $|F|$ from the original data in white-beam diffraction, it is necessary to make wavelength-dependent corrections for the incident spectrum $\mathcal{I}_0(\lambda)$, absorption and extinction. Although the correction methods of the former two terms seem to be established so far, there has not been much discussion about the extinction effect. As demonstrated by Niimura, Tomiyoshi, Takahashi & Harada (1975), however, the extinction effect is very important in white-beam diffraction because a wide range of wavelengths of the incident radiation, sometimes more than 1 Å, is often used and, due to a $\lambda^4$ dependence of the integrated intensity, wavelength variation of the extinction effect is very large.

The extinction theories proposed hitherto have been developed by assuming a monochromatic incident beam and there has not been much discussion about the application of the theories to a white-beam radiation experiment. The purpose of the present paper is to clarify this point. As the theory of extinction, the formulation developed by Zachariasen (1967) is widely used but it includes a mathematical mistake. Becker &

0567-7394/80/040600-05$01.00 